AVERAGE AND WORST-CASE SPECIFICATIONS OF PRECIPITATING AURORAL ELECTRON ENVIRONMENT

David A. Hardy, William J. Burke, and M. S. Gussenhoven
Air Force Geophysics Laboratory
Hanscom Air Force Base, Massachusetts 01731

E. Holeman
Emmanuel College
Boston, Massachusetts 02115

H. C. Yeh
Boston College
Chestnut Hill, Massachusetts 02167

The precipitating electrons in the auroral environment are highly variable in their energy and intensity in both space and time. As such they are a source of potential hazard to the operation of the Space Shuttle and other large spacecraft operating in polar orbit. In order to assess these hazards both the average and extreme states of the precipitating electrons must be determined. In this paper we present work aimed at such a specification. In the first half of the paper we present results of a global study of the average characteristics. In this study the high latitude region was divided into spatial elements in magnetic local time and corrected geomagnetic latitude. The average electron spectrum was then determined in each spatial element for seven different levels of activity as measured by K_p using an extremely large data set of auroral observations. In the second half of the paper we present a case study of an extreme auroral electron environment in which the electrons are accelerated through a field aligned potential as high as 30,000 volts and in which the spacecraft is seen to charge negatively to a potential approaching .5 kilovolts.

INSTRUMENTATION

The data used for this analysis were from the SSJ/3 detectors on the F2 and F4 satellites and the SSJ/4 detector on the F6 satellite of the Defense Meteorological Satellite Program as well as the CRL-251 experiment on the P78-1 satellite of the Space Test Program. The SSJ/3 detectors consisted of a set of two curved plate electrostatic analyzers capable of measuring the flux of precipitating electrons in 16 energy channels between 50eV and 20,000 eV. The SSJ/4 detector consists of a set of four curved plate electrostatic analyzers that measure both electrons and ions in 20 energy channels each,

in the energy range from 30 eV to 30000 eV. Both the SSJ/3 and SSJ/4 detectors return a full spectrum over all energy channels once per second and all detectors are oriented on the spacecraft such that they look towards the local zenith. The CRL 251 experiment consists of two SSJ/3 detectors mounted at right angles with their look directions in the spin plane of the satellite. Each detector returns 4, 16 point spectra each second. The satellite has a spin rate of approximately 11 RPM with the spin plane in the orbit plane of the satellite.

All the satellites were launched into circular sun synchronous orbits. The F2 satellite's orbit plane was initially in the dawn-dusk meridian but precessed towards the 0830-2030 MLT meridian during the satellite's lifetime. The period for which data are available, the altitude of the orbit, and the orbital plane are listed in Table 1.

The DMSP sensors are operated continuously and approximately 80% of the data were available for this study. For the P78-1 approximately 1000 polar passes were available from 1979. For the determination of the average characteristics, the F2, F4, and P78-1 data were used. The worst case study was performed using the F6 data since these data cover a wider range in energy.

AVERAGE CHARACTERISTICS

Historically, there have been two approaches to global specification of the average characteristics of auroral precipitation. In the first of these the researcher builds up a global or local time picture using a set of individual passes each studied in detail (ref 1 & 2). The advantage of such an approach is that all the details of each pass are considered in creating an overall picture. The major disadvantage in such studies is that in order to keep both the analysis and data presentation manageable the researcher must restrict the total number of passes studied either by spacing them widely in magnetic local time or in activity. In the second approach the researcher builds up his global picture by dividing the region of interest into zones in magnetic local time, geomagnetic latitude and activity he then uses very large data sets to determine the average value of the quantity of interest in each zone (ref 3 through 9). This approach has the advantage of providing real global maps. It's major disadvantage is that in the averaging process all small spatial and temporal variations are smoothed out, of necessity. The number of such studies done in the past has additionally been restricted by the fact that they require very large data sets (millions of samples) and they require significant amounts of computer time.

In this study we have taken the second of these two approaches using the data set from identical electrostatic analyzers flown on three Air Force satellites. We divided the high latitude region into zones in magnetic local time and corrected geomagnetic latitude. In MLT the divisions were 48 one half hour sections. In latitude there were 30 divisions at 2^{0} increment between 50 and 60 degrees, 1^{0} increments between 60 and 80 degrees, and 2^{0} increments from 80 to 90 degrees. Seven such matrices were created, one for the Kp = 0, 0+ cases, one for Kp = 1-, 1, 1+ cases and so on up to Kp = 5-, 5, 5+. The last matrix included all cases greater than Kp = 6-. Fifteen months of data were used from the F-2 and F-4 satellites. The fifteen months were chosen to give an even distribution of the data over the seasons of the year and to provide sufficient coverage at high activity. Altogether the 15 months

of data provided 13.6 million spectra. All orbits of the P78-1 satellite in the interval from February 1979 to January 1980 were used. This comprised approximately .52 million additional spectra. The 14.1 million spectra were divided among the 7 levels of Kp as follows; Kp = 0, 7.85%; Kp = 1, 23.82; Kp=2, 26.9%, Kp = 3, 21.9%; Kp = 4, 10.5%; Kp = 5, 5.3%; Kp > 6-, 3.6%. In each zone the average and standard deviation of the differential number flux for each of the 16 energy channels of the detector was calculated using all spectra that fell within that zone. The final product is therefore the average spectrum in each zone at each level of activity.

From the average spectra we calculated integral quantities over the entire energy range of the average energy spectrum. The three quantities calculated were the integral number flux in units of e/cm^2-sec-ster defined as:

$$JTOT = j(E_1)\,(E_2 - E_1) + \sum_{i=2}^{15} j(E_i)\frac{(E_{i+1} - E_{i-1})}{2} + j\,(E_{16})\,(E_{16} - E_{15})$$

The integral energy flux in units of keV/cm^2-sec-ster defined as:

$$JETOT = E_1\, j(E_1)\,(E_2 - E_1) + \sum_{i=2}^{15} j(E_i)\, j(E_i)\frac{(E_{i+1}) - E_{i-1})}{2} +$$

$$E_{16} j\,(E_{16})\,(E_{16} - E_{15})$$

and the average energy

$$EAVE = JETOT/JTOT$$

where

$j(E_i)$ = the average differential flux in the ith energy channel

E_i = the central energy of the ith channel

These three quantities are displayed as isocontour maps in Figures 1a-d, 2a-d, and 3a-d where we have plotted the Kp = 0, 2, 4, and 6 cases. The discussion of these maps is in two sub-sections; the first dealing with the characteristics of the relatively hot electron (EAVE > 600 eV) and the second dealing with the characteristics of the colder electrons. Such a division is made based on a comparison of the maps of integral flux and average energy. Such a comparison shows that the high latitude region separates naturally into two regions based upon the average energy of the electrons. The hotter plasma is confined to a roughly annular region whose low latitude edge is the equatorward edge of the auroral zone while the colder plasma fill the remaining area between the poleward edge of the annulus and the geomagnetic pole. The colder electron region is composed of a band of relatively intense precipitation bounding the poleward edge of the hot plasma and a region of lower intensity precipitation in the rest of the area up to the pole.

HOT ELECTRON REGION

For the hot electrons we note the following:

1) The average energy of the precipitating electron varies greatly in magnetic local time. In general the peak average energies are highest on the morning side of the oval. Within the morning side region there are two maxima in the average energy; one between midnight and 0600 MLT and the second typically two hours pre-noon. In tables 2a and 2b the location and electron characteristics for the two maxima are listed for all seven Kp zones.

One notes that the average energy of the post midnight maximum is between 3 and 5 keV in a latitude range between 63 and 67°. The local time of these maxima varies over 6 hours and the trend is for the energy flux to increase with increasing Kp. The lack of a post midnight maximum for the Kp=5 case we attribute to the relatively limited sampling provided by the P78-1 satellite in this region and at this level of activity. The pre-noon maximum is more fixed in magnetic local time and more ordered by Kp. Except for Kp=0 case this maxima is always found between 0930 and 1100 MLT and at a geomagnetic latitude that smoothly decreases with increasing Kp. The average energy increases from Kp=0 to Kp=3 but then decreases for all higher Kp reaching a value for the highest activity case a factor of two below that of the Kp=0 ease. In a similar manner the energy flux increases from Kp=0 to Kp=3 but then is approximately stable for all higher activities.

2. At energies above 1 keV the region of hot plasma is not continuous about the oval. For Kp=0 the average energy does not reach 1keV at any latitude in the MLT range from ~ 1800 to 2200. For the Kp=1 and 2 cases there is a minimum within the region of hot plasma at approximately 1800 hour MLT. For the four remaining cases there is a clear minimum between noon and 1800 hours MLT. The average energy of this minimum falls below 1 keV. For the four highest activity cases the location of the minimum appears to move to earlier local times with increasing activity. Part of this effect appears to result from a change with activity in the magnetic local time past noon to which hot electrons drifting around on the morning side are able to penetrate. These electrons are seen at the latest MLT for Kp=0 and penetrate to progressively earlier MLTs with increasing activity. For the Kp ≥6- case there are few regions to the dayside of the dawn-dusk meridian in which the average energies reaches 1.5 keV.

3. The majority of the energy flux of particles into the high latitude region is carried by the hot electrons. Typically for any MLT zone on the nightside of the oval the latitude of the maximum in energy flux is near or coincides with the maximum in average energy. At all activity levels above Kp=0 the isocontours of energy flux within the hot electron region have a C or horseshoe shape that is roughly symmetric about a meridian one to two hours post midnight and post-noon. The maximum energy flux occurs slightly before midnight for Kp=0 and 1 but is clearly post midnight for all higher activity cases.

4. The energy flux into the nightside oval and up to approximately 1000 MLT on the dayside increases with increasing activity as the oval expands. By contrast the energy flux carried by hot electrons at noon reaches a maximum

at Kp=? and then decreases for higher activity. This is shown in Table 3 where we have listed the maximum energy flux and it's latitude for the 0000 to 0030 MLT zone and for the peak in average energy for the hot electrons in the 1130 to 1200 MLT zone.

The latitude for both cases decreases for increasing activity as would be expected from the overall movement of the oval equatorward. The energy flux at midnight increases by more than an order of magnitude from Kp=0 to Kp >6- while the energy flux at noon reaches a maximum value of 7.79×10^7 keV/ cm^2-sec-ster for Kp=? and then decreases for increasing Kp above this point, reaching a value for the Kp>6- case approximately a factor of two lower than the Kp=0 case. The ratio of the energy flux at midnight to that at noon increases with increasing Kp except for the Kp=5 case. The 7 values from Kp=0 to Kp>6- are ?.7, 4.1, 4.7, 12.0, 21.5, 18, 72.5.

COLD ELECTRON REGION

For the cold electrons (EAVE < 600 eV) we note the following:

1. The highest number flux of cold electrons is found within the dayside portion of the overall region of electron precipitation. At the first five activity levels there is a clear crescent shaped region of cold electrons roughly symmetric about noon or slightly skewed towards prenoon. The crescent shaped region is most clearly evident in the Kp=0 and Kp=1 cases where at a level of above 5×10^7 electrons/cm^2-sec-ster it extends in magnetic local time over the entire dayside region and one to several hours into the nightside region. The region extends closer to midnight on the morning side than the evening side. The same behavior is maintained for the next three levels of activity but is obscured in the isocontour plots by the increasing integral flux on the night side from the hot electrons. For the two highest activity cases there is still an extended region of low energy precipitation on the dayside but it is not as well organized as for the lower activity cases.

2. The intensity of the integral number flux within the dayside region shows little if any increase with increasing activity. Except for the Kp > 6- case the integral number flux is typically between 5×10^7 and 2×10^8 electrons /cm^2-sec-ster. Although the level of flux within the region is relatively constant the total flux of electrons into the region is increasing with increasing activity. For the 7 levels of activity the total downcoming flux over the entire dayside with energies between 50 eV and 660eV are 7.65×10^{24}, 8.89×10^{24}, 1.0×10^{25}, 1.21×10^{25}, 1.56×10^{25}, 1.97×10^{25} and $3.78 \times 10^{?}$electrons/ -sec-ster. These numbers were obtained by determining the integral flux for electrons with energies between 50 eV and 660 eV in each spatial element on the dayside multiplying these by the area of the spatial element and summing. For all but the Kp> 6- case this trend is well fit by the equation,

$$I = 7.8 \times 10^{24} \, e^{\cdot 2Kp} \text{ electrons/sec-ster}$$

3. Within the dayside region of cold electron precipitation there is, in all but the Kp> 6- case, a clear prenoon maximum. In Table 4 the parameters for these maxima are listed.

One notes that the maximum's location in MLT is relatively constant while the latitude decreases with increasing activity as the oval expands. The integral number flux increases only from 3.05 to 4.1 x 10^8 from the Kp=0 to the Kp> 6- case. Both the integral energy flux and average energy are similarly within a narrow range except at the two highest activities. These increases at higher activity are attributable to an increase in the spatial variability of the oval such that some hot electron spectra have been used to determine the average spectrum from which the energy flux and average energy were calculated If at all activity levels the values listed in Table 3 are recalculated using only the portion of the spectrum between 50eV and 660eV the values for the Kp=0 to Kp=3 cases vary by less than 10% for all three quantities. For Kp=4 and 5 cases, however, the energy flux drops to values below 10^8 keV/cm^2-sec-ster and the average energy to values below 200 eV.

4. In the dayside region of cold electrons there is a clear minimum in average energy. The location and electron characteristics at the minimum are listed in Table 5.

The location in latitude shows a total variation of 5^0 with activity and except at high activity is found between 1100-1200 MLT. Again the electron characteristics are quite stable with increasing activity. The integral number flux ranges between 3 and 10 electrons/cm^2-sec-ster except for the KP > 6- case. The integral energy flux value falls in a similar narrow range and the average energy shows a slight decrease with increasing activity. These average energy minima sit near the poleward edge of the cresent shaped region of cold electron precipitation.

WORST CASE ENVIRONMENT

The concept of a worst case environment for large space structures in near-earth, polar orbit involves an extrapolation of experience with small satellites near geostationary altitude. The need for extrapolation derived from our historical situation which presents many well-documented examples of severe charging at geostationary altitude, a few cases of small-satellite changing at ionospheric altitudes, and as yet no experience with large structures, such as Shuttle, in polar orbit. At geostationary altitude the worst charging occurs when satellites are in the shadow of the earth during some substorm injection events. In this situation the occurrence of charging is unambiguously determined by the location in energy of the so-called "charging peaks" in the positive ion spectrum. If a satellite charges to - 5kV, low-energy ions in the vicinity of the satellite are accelerated through this potential. Typically, a large flux of ions would be measured in the energy channel centered nearest 5KeV while few if any ions would be detected in energies channels below this value. Mullen and Gussenhoven (ref 10) (1982) found that the most severe charging occurs during those substorm injection events that are characterized by strong fluxes of electrons with energies above 10 keV. Impacting electrons with energies above (below) this value produce less (more) than one secondary electron per particles for typical spacecraft materials (ref 11) With this criterion in mind Hardy (ref 12) surveyed more than 10,000 passes of DMSP/F2 over the auroral zone to identify conditions under which the flux of electrons with energy > 1 keV exceeded 10^{10} electrons/cm^2-sec-ster. Although these energetic electron observations are useful for modelers who require realistic, worst-case fluxes it provides no empirical guidelines as to what degree the satellites actually charge.

With the launch of DMSP/F6 in December 1982 it has become possible to specify the degree to which charging occurs in "worst case" auroral environments. This satellite carried detectors capable of measuring the fluxes of downcoming electrons and positive ions with energies between 30 eV and 30 keV. The satellite also carried detectors to measure the densities and temperatures of thermal ions and electrons. Because the geometric factor of the energetic ion detector greatly exceeds that of any previously flown, it is possible for the first time, to look for ion "charging peaks" as indicators of spacecraft charging in the ionosphere. The detector systems as well as the methods for data presentation and identifying severe charging events are described in a companion paper (ref 13) and will not be repeated here.

Figures 4 and 5 give the average energies (top panels), directional energy flux (middle panels) and directional number flux of electrons and positive ions measured during a northern, high-latitude pass of DMSP on 12 January 1983. The data are presented as a function of UT in seconds of the day, geographic latitude and longitude; magnetic latitude, longitude and local time. Attention is directed to the two minute interval between 35820 (0957) and 35940 (0959) UT. The electron flux rose sharply from typical polar rain values of 2×10^6/cm^2-sec-ster, starting at 35860 UT to a maximum value of 10^{10}/cm^2-sec-ster at 35878 UT. The flux level then decreased to a nearly steady value of 5×10^8 for the following minute. The average energy profile suggests that the satellite either passed through two closely spaced inverted-V structures or through a single, complex inverted V with a very intense substructure at its poleward boundary. During the subinterval 35860-35880 UT, the ion flux increased by three orders of magnitude with no easily recognized increase in average ion energy. An intense flux of high-energy electrons accompanied by an increased flux of low-energy ions is often an indicator of spacecraft charging at geostationary altitudes (ref 14). An analysis of individual distribution functions for ions and electrons, presented below, shows that this can also be regarded as a signature of charging at ionospheric altitudes. Before examining individual spectral measurements two additional comments related to Figures 4 and 5 should be made. First, during the interval 35880 to 35940 as the satellite passed through the equatorward (portion of the)inverted V the flux of ions remained constant at ~ 10^6 /cm^2-sec-ster and their average energy increased to several kilovolts. As demonstrated below no measurable charging occurred during this interval. Second, the electron flux levels of 10^{10}/cm^2-sec-ster near 35875 UT represent lower bounds on the actual flux. The integrations are performed only over the finite energy range (30 eV - 30 keV) of the sensor.

Figures 6 a-f give six examples of phase space densities for electrons and ions with energies between 30 eV and 30 KeV as measured by DMSP/F6 in crossing the inverted V structure(s). Before examining the measurements it should be recalled that both the electron and ion detectors consist of two analyzers. The low (high) energy analyzer covers the range 30 eV to 1 keV (1 to 30 keV) in 10 logarithmically spaced steps. Each of the analyzers steps from high to low in energy. Thus, the 1 keV sample of the low-energy analyzer occurs almost a full second before the 1 keV sample of the high energy analyzer. In rapidly varying environments the 1 keV measurements of the two analyzers can be quite different. In smoothly varying regions measured fluxes agree within normal, statistical fluctuations. The different values of electron distribution functions at 1 keV, in the examples given in Figure 6 reflect rapid spatial-temporal variations in the environment rather than a calibration deficiency in the instrument.

The electron and ion distribution functions in Figure 6 were chosen to illustrate conditions leading to weak (a,f), moderate (c,e) and strong (b,d) spacecraft charging. To help identify the degree of charging expanded plots of the low energy portions of ion-distributions appear as insets. At 0957:48 UT as the satellite entered the inverted V the ion distribution decreases monotonically indicating that the satellite potential was greater than or equal to - 30 V. One second later the electron distribution hardened considerably and the low-energy portion of the ion distribution shows a peak at 300 eV indicating a vehicle potential of -300 V (ref. 13). The rapidity with which the vehicle potential fluctuates is shown in examples c (0957:56) d (0957:58) and e (0957:59) where the charging peak is seen at 100 eV, 440 eV and 44 eV, respectively. We note that, at 0957:58 UT in the energy range 9 to 30 keV, the electron distribution function is monotonically increasing. If we assume that the auroral electrons have undergone a field-aligned acceleration between the magnetosphere and ionosphere, then the detected electrons are secondary and degraded primaries. The potential drop above the ionosphere is at least 30 kV. The primary electron beam has an energy greater than 30 keV; beyond the energy sensitivity of the DMSP/F6 detection range. The final example at 0958:06 UT comes from the equatorward inverted-V. Although the primary electron beam has been accelerated through a potential of 14 kV, the ions have a monotonically decreasing distribution. Potentials > - 30 V are typical of this equatorward inverted-V encounter.

The control of spacecraft charging exerted by energetic electrons is illustrated in Figure 7. The top panel gives the directional flux of electrons with energies > 5 keV (dashed line) and > 10 keV (solid line). As just mentioned the flux measured at 0957:58 (35878) UT is lower bound on the actual flux. The satellite potentials inferred from the measured ion distribution functions appear in the bottom panel. We see that there are one for one variations in the energetic electron flux and the satellite potential. The degree of charging achieved at geostationary altitude in a given energetic particle environment exceeds that expected for satellites in the ionosphere. In the ionosphere severe charging effects should be mitigated due to currents carried by relatively dense, cold ions. Simultaneous measurements from the thermal plasma probes in the vicinity of the inverted-V event(s) are presented in Figure 8. Data are presented as densities of thermal electrons (top panel) and ions (bottom panel) determined while the detectors operated in the constant bias Mode 1 (ref 13). A positive bias on the outer grid of the electron sensor is responsible for the factor of two greater electron than ion density prior to 0957 and after 0959 UT. Note that between 0956 and 0957 UT the electron and ion densities decreased by a full order of magnitude. This density decreased occurred prior to the first encounter with the inverted V. Beginning at 0957:30 the current to the electron sensor decreased by more than another order of magnitude. Because the ions show the opposite response we attribute the thermal electron current suppression as due to the increase satellite charging encountered at this time.

In the companion paper, Burke and coworkers (ref 13) presented another example of severe charging by DMSP. In this event the satellite potential only reached -65V. The present case differs in two significant ways. First, although the inverted V electron flux levels were comparable, the average energies were significantly larger in the present case. Second, the thermal plasma density was an order of magnitude higher in the case presented by

Burke and coworkers. This means that there is roughly an order of magnitude less ion current available to neutralize the current due to energetic electrons. It would appear that both energetic electrons and a cold plasma depletion are required for satellites at ionospheric altitude to acquire the high degree of charging observed by DMSP on January 12, 1983.

REFERENCES

1. Winningham, J.D., F. Yasuhara, S.-I. Akasofu and W.J. Heikkila, (1975), The Latitudinal Morphology of 10eV to 10 keV Electron Fluxes during Magnetically Quiet and Distrubed Times in the 2100 - 0300 MLT Sector, JGR, 80, 3148.

2. Lui, A.T.Y., D. Venkatesan, C.D. Anger, S. -I. Akasofu, W.J.Heikkila, J.D. Winningham and J.R. Burrows, (1977), Simultaneous Observations of Particle Precipitation and Auroral Emissions by the ISIS 2 Satellite in the 1900 - 2400 MLT, Sector, JGR, 82, 1977.

3. Feldstein, Y.I., (1966), Peculiarities in the Auroral Distribution and Magnetic Disturbances Distribution in High Latitudes Caused by the Asymmetrical Form of the Magnetosphere, Planet. Space Sci, 14, 121.

4. Sharp, R.D. and R.G. Johnson, (1968), Some Average Properties of Auroral Electron Precipitation as Determined from Satellite Observations, JGR, 73, 970.

5. Eather, R.H. and S.B. Mende, (1971), Airborne Observations of Auroral Precipitation Patterns, JGR, 76, 1746.

6. Starkev, G.V. and Y.I. Feldstein, (1971), Substorm in Auroras, Geomagn. Aeron., 11, 478.

7. McDiarmid, I.B., J.R. Burrows and E.E. Budzinski, (1975), Average Characteristics of Magnetospheric Electrons (15 eV to 200 keV) at 1400 km, JGR, 80, 73.

8. Walis, D.D. and E.E. Budzinski, (1981), Empirical Models of Height Integrated Conductivities, JGR, 86, 125.

9. Spiro, R.W., P.H. Reiff and L.J. Maher, Jr., (1982), Precipitating Electron Energy Flux and Auroral Zone Conductances - An Empirical Model, JGR, 87, 8215.

10. Mullen, E. G., and Gussenhoven, M. S. (1982) High-Level spacecraft charging environments near geosynchronous orbit, AFGL-TF-82-0063 Hanscom AFB, MA 01731.

11. Lamframboise, J. G., Godard, R., Kamitsuma, M. (1982) Multiple floating potentials, "threshold temperature" effects, and "barrier" effects in high-voltage charging of exposed surfaces on a spacecraft" in Proceedings of International Symposium on Spacecraft Materials in Space Environment, Toulouse France, 8-11 June 1982, Publications Branch ESD, Noordwijk, The Netherlands.

12. Hardy, D. A. (1983) The worst case, charging environment, in Proceeding of AFGL Workshop on Natural Charging of Large Space-Structures in Near-Earth Polar Orbit: Sept 14-15, 1982, ed by R. C. Sagalyn, D. E. Donatelli and I. Michael, AFGL-TR-83-0046, Hanscom AFB, MA 01731.

13. Burke, W. J., Hardy, D. A., Rich, F. J., Rubin A. G., Tautz, M. F. Saflekos, N. A. and Yeh, H. C., (1984), Direct measurements of severe spacecraft charging in the auroral ionosphere, Proceedings of Spacecraft Environment Interactions Conference (this volume).

14. DeForest, S. E., (1972) Spacecraft Charging at Synchronous Orbit, JGR, 77, 651-659.

Table 1

Satellite	Orbital Plane	Altitude	Data Availability
F2	0600 - 1800	840 Km	9/77 - 2/80
F4	1030 - 2230	840 Km	6/79 - 8/80
P78-1	0000 - 1200	600 Km	3/79 - present
F6	0600 - 1800	840 Km	12/82 - present

Table 2a
Post Midnight Maximum

Kp	Average Energy	Energy Flux	Magnetic Latitude	MLT
0	3.41 KeV	8.27×10^7 KeV/cm^2-sec-ster	67°	0400-0430
1	4.71 "	7.65×10^7 "	66°	0530-0600
2	3.78 "	3.90×10^8 "	65°	0130-0200
3	3.93 "	6.98×10^8 "	65°	0130-0200
4	3.46 "	7.10×10^8 "	66°	0000-0030
5	---	---	---	---
>6-	5.87 "	1.67×10^9 "	63°	0230-0300

Table 2b
Pre Noon Maximum

Kp	Average Energy	Energy Flux	Magnetic Latitude	MLT
0	2.97 KeV	2.16×10^7 KeV/cm^2-sec-ster	71°	1400-1430
1	3.90 "	6.34×10^7 "	70°	0930-1000
2	5.68 "	1.07×10^8 "	70°	1030-1100
3	6.40 "	1.38×10^8 "	69°	1000-1030
4	5.02 "	9.42×10^7 "	67°	1000-1030
5	4.81 "	1.33×10^8 "	66°	0930-1000
>6-	1.80 "	1.06×10^8 "	65°	0930-1000

Table 3

	0000 - 0030 MLT			1130 -1200 MLT		
Kp	Max. Energy Flux		C.G. Latitude	Energy Flux		C.G. Latitude
0	1.04×10^8	KeV/cm^2-sec-ster	69°	3.75×10^7	KeV/cm^2-sec-ster	72°
1	1.90×10^8	"	68°	4.55×10^7	"	71°
2	3.69×10^8	"	66°	7.79×10^7	"	71°
3	6.64×10^8	"	65°	5.50×10^7	"	69°
4	7.75×10^8	"	66°	3.51×10^7	"	67°
5	4.67×10^8	"	62°	2.61×10^7	"	66°
>6-	1.37×10^9	"	62°	1.92×10^7	"	64°

Table 4

Prenoon Integral Number Flux Maximum

Kp	Lati-tude	MLT	Integral Number Flux		Integral Energy Flux		Average Energy
0	79°	0800-0830	3.05×10^8	e/cm^2-sec-ster	7.04×10^7	e/cm^2-sec-ster	232eV
1	78°	0800-0830	3.22×10^8	"	8.45×10^7	"	272eV
2	78°	0930-1000	3.32×10^8	"	8.43×10^7	"	256eV
3	77°	1100-1130	3.80×10^8	"	7.03×10^7	"	187eV
4	74°	0830-0900	3.61×10^8	"	1.95×10^8	"	552eV
5	73°	0830-0900	4.10×10^8	"	1.66×10^8	"	465eV

Table 5

Average Energy Minimum

Kp	Latitude	MLT	Integral Energy Flux		Average Energy
0	81°	1100-1130	4.57×10^7	KeV/cm^2-sec-ster	199 eV
1	81°	1130-1200	4.88×10^7	"	183 eV
2	81°	1130-1200	3.63×10^7	"	168 eV
3	79°	1100-1130	4.44×10^7	"	165 eV
4	78°	1130-1200	3.96×10^7	"	162 eV
5	78°	1230-1300	3.18×10^7	"	147 eV
> 6-	76°	1200-1230	7.29×10^7	"	184 eV

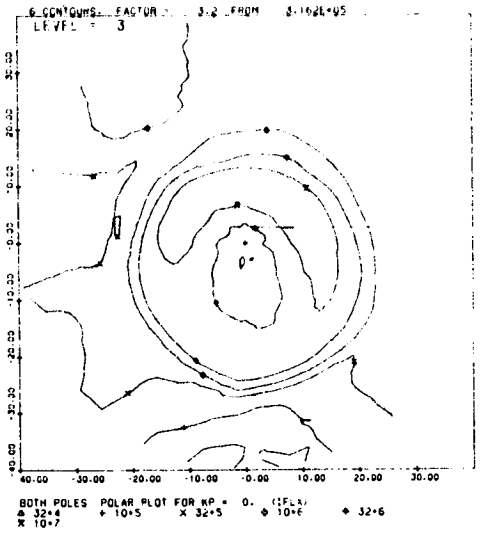

A

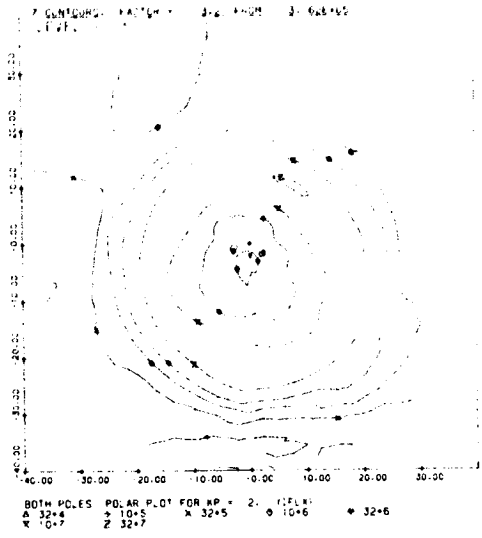

B

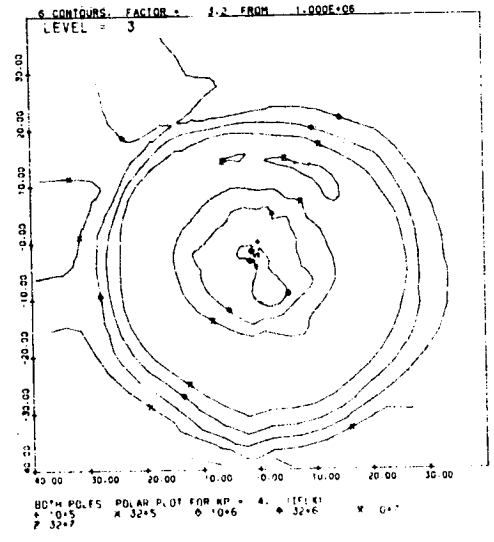

C

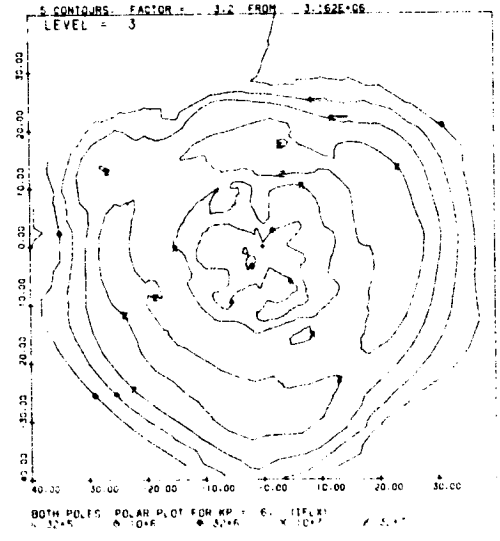

D

Figure 1. - Isocontour maps of the integral number flux (IFLX) of precipitating electrons in units of electrons/cm^2 sec sr for the four activity levels K_p=0, 2, 4, and $\geq$6-. The plots are in a corrected geomagnetic latitude - magnetic local time coordinate system. The geomagnetic pole is marked by a cross (+). Midnight magnetic local time is centered at the bottom of each figure, noon at the top.

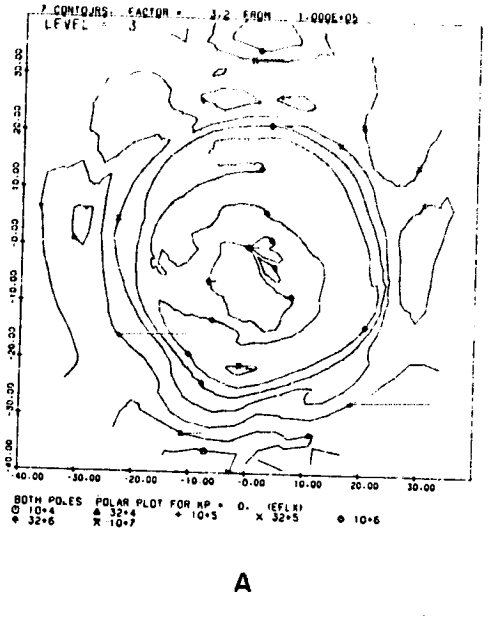

A

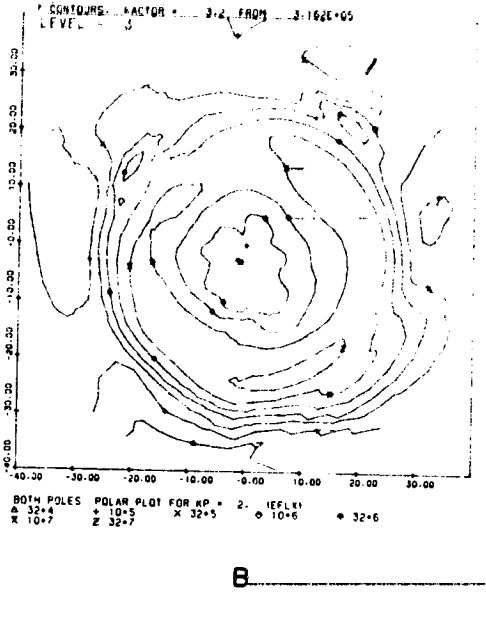

B

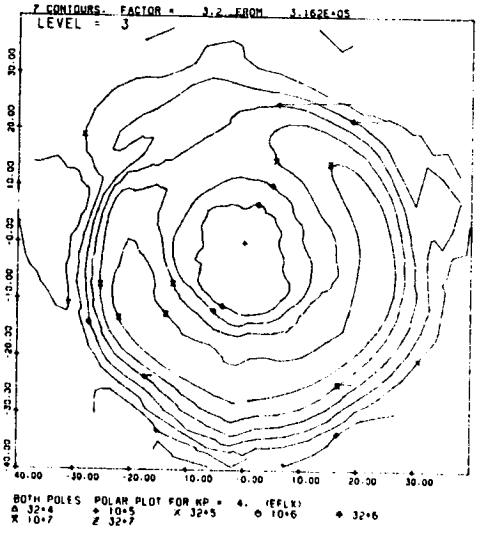

C

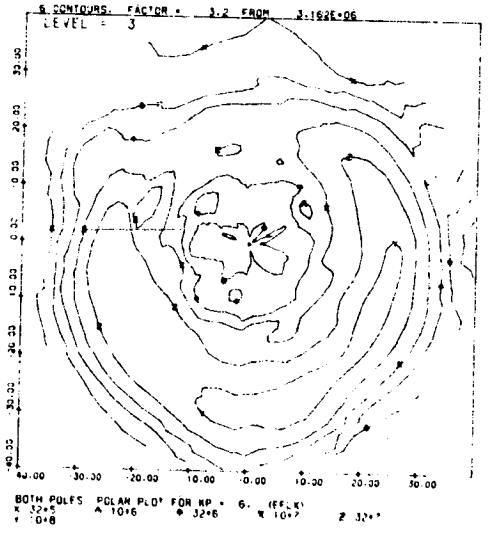

D

Figure 2. - Isocontour maps as in figure 1 for the integral energy flux (EFLX) of precipitating electrons in units of keV/cm^2 sec sr.

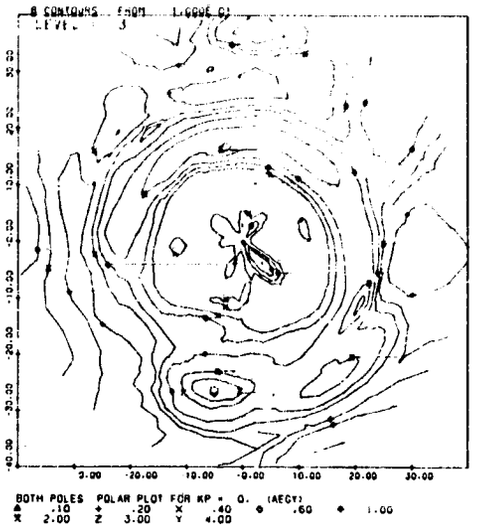

A

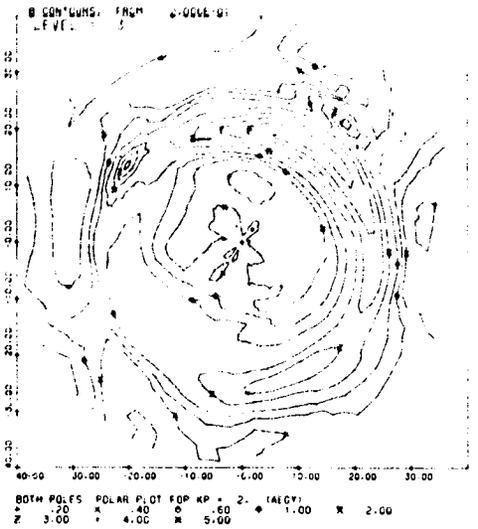

B

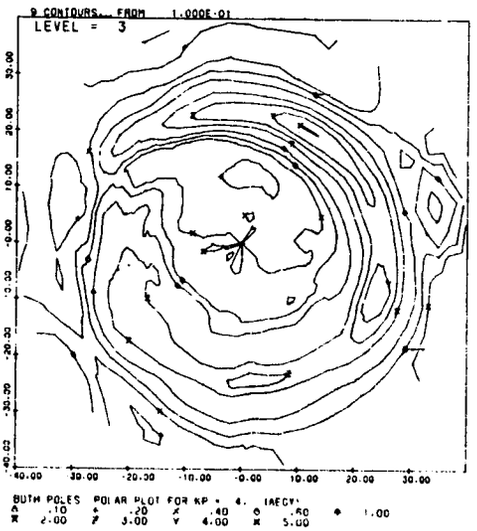

C

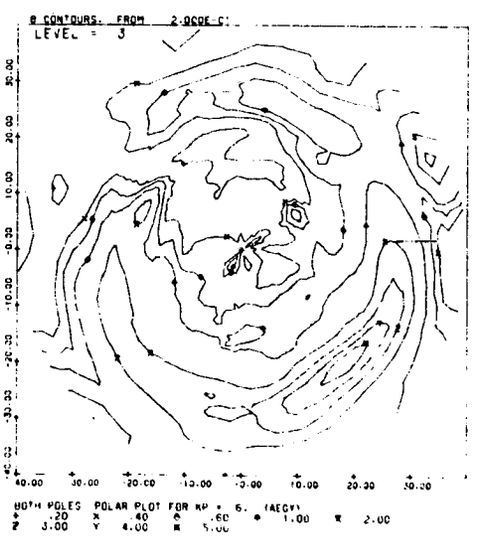

D

Figure 3. - Isocontour maps as in figure 1 for the average energy (AEGY) of precipitating electrons in units of keV.

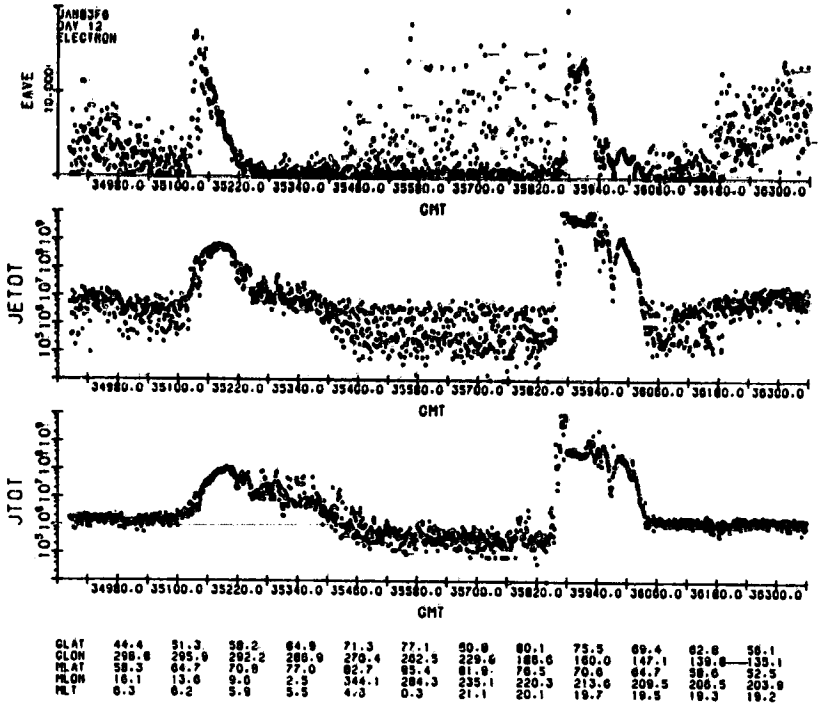

Figure 4. – Average energy, directional energy flux, and directional number flux of downcoming electrons with energies between 30 eV and 30 keV.

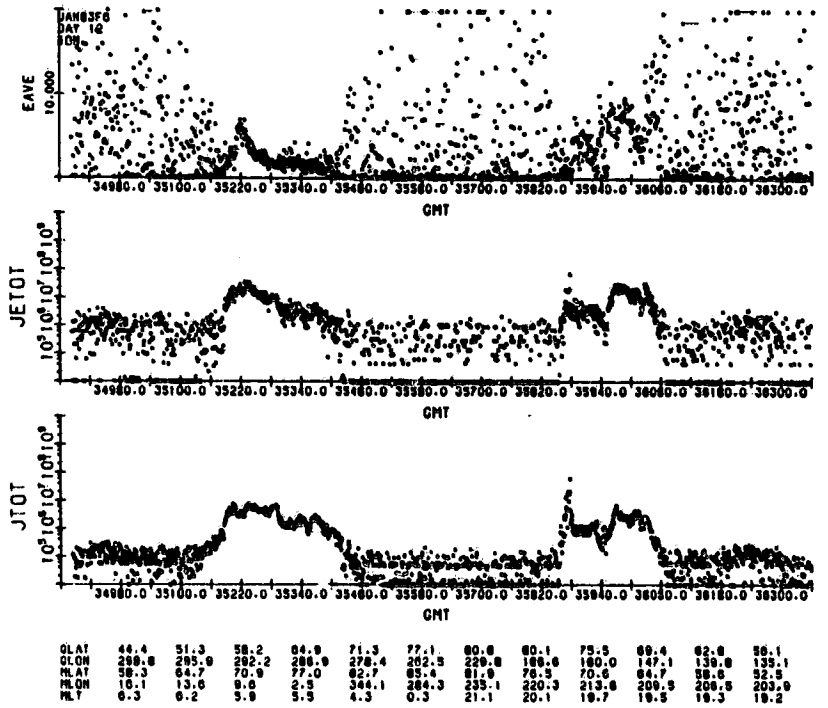

Figure 5. – Average energy, directional energy flux, and directional number flux of downcoming ions with energies between 30 eV and 30 keV.

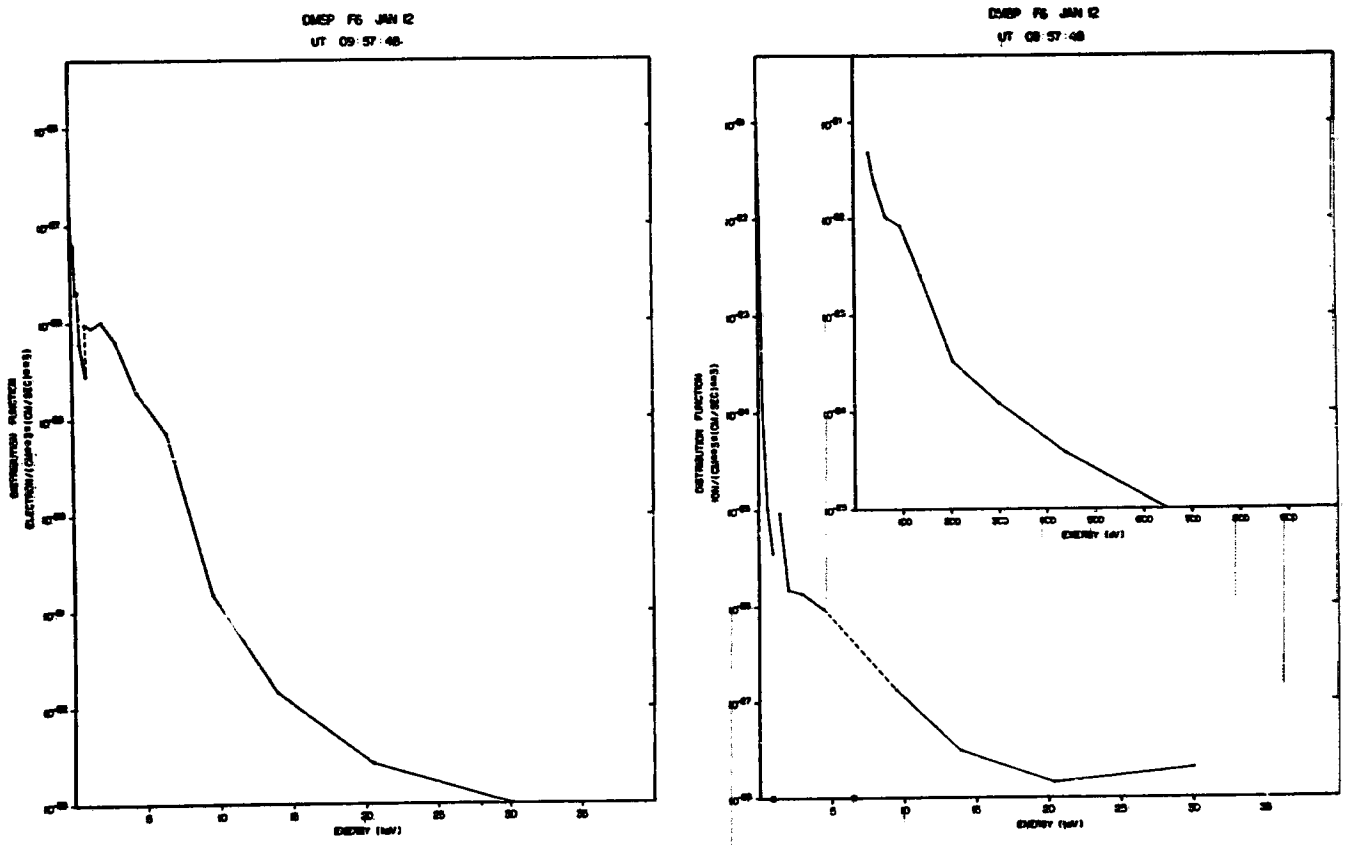

(a) At 09:57:48 UT.

Figure 6. – Distribution functions of electrons and ions with energies between 30 eV and 30 keV as measured on 12 January 1983 by DMSP/F6.

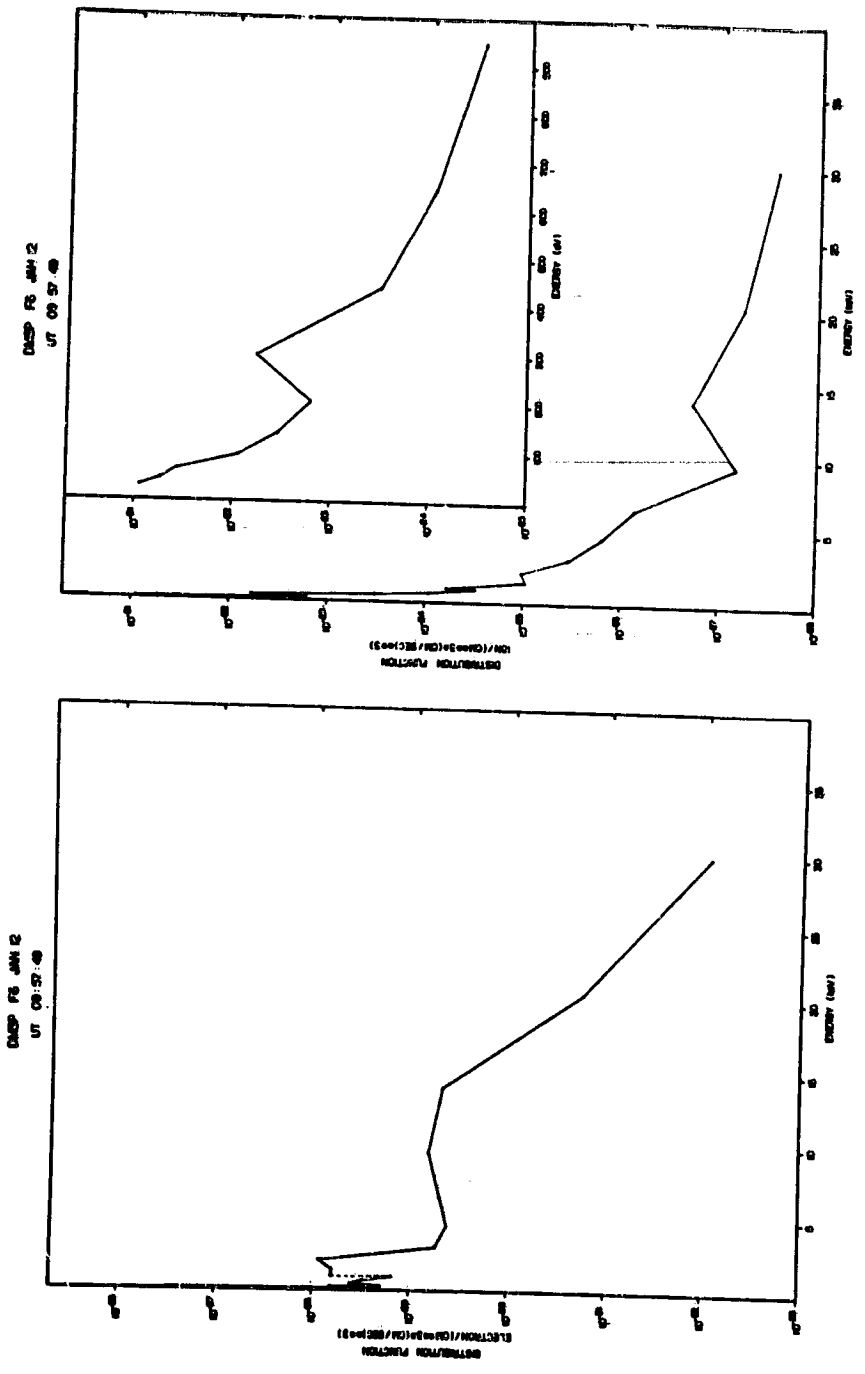

(b) At 09:57:49 UT.

Figure 6. - Continued.

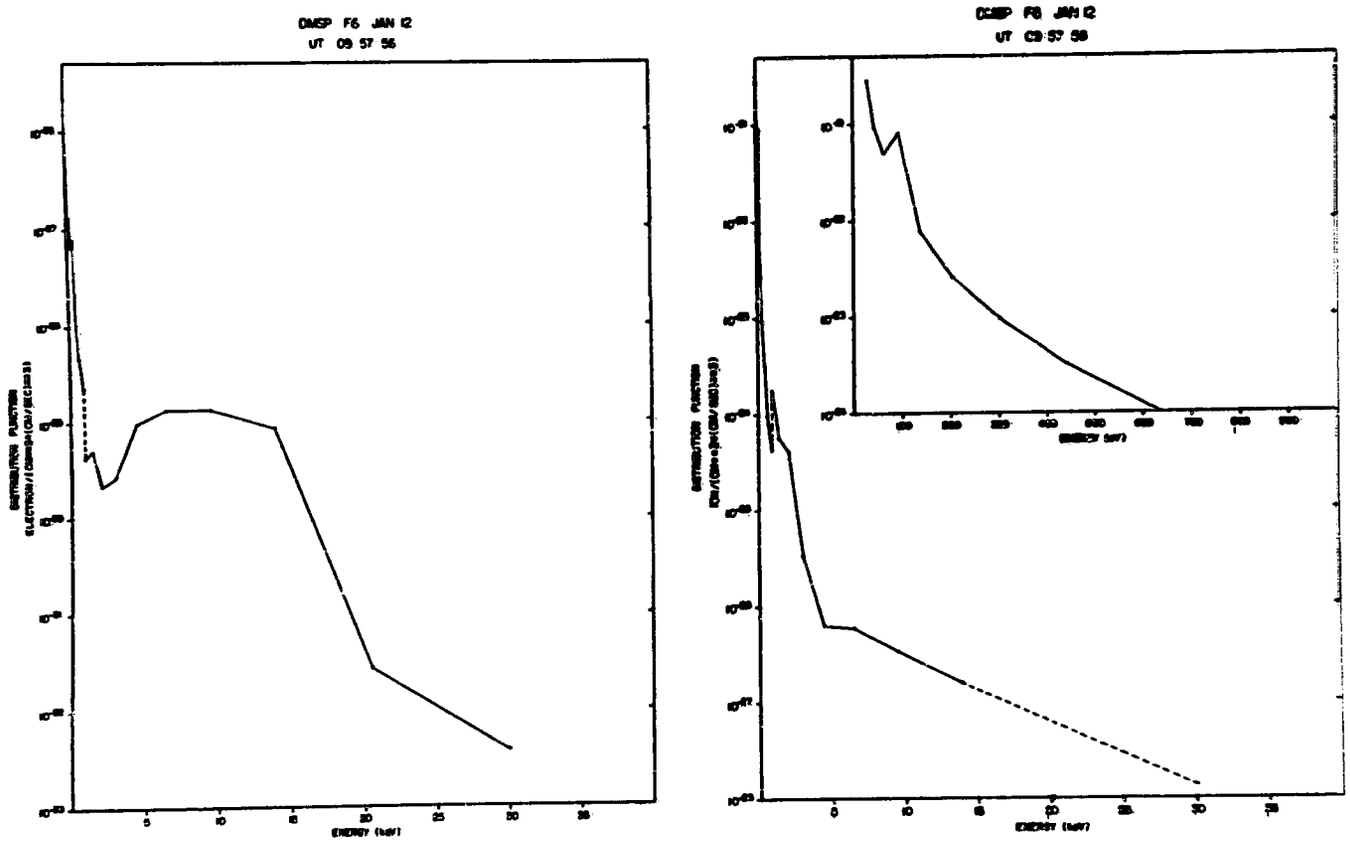

(c) At 09:57:56 UT.

Figure 6. - Continued.

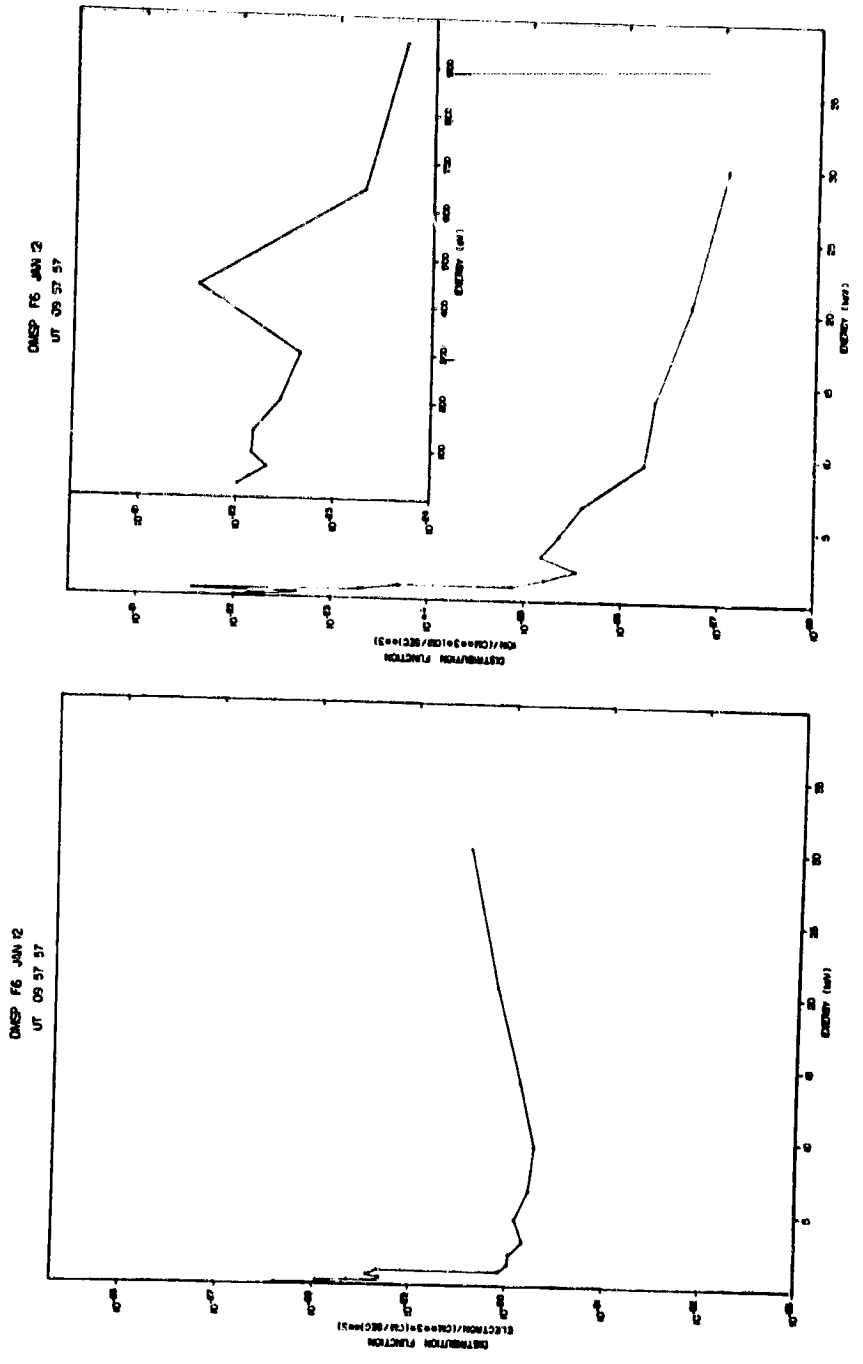

(d) At 09:57:57 UT.

Figure 6. - Continued.

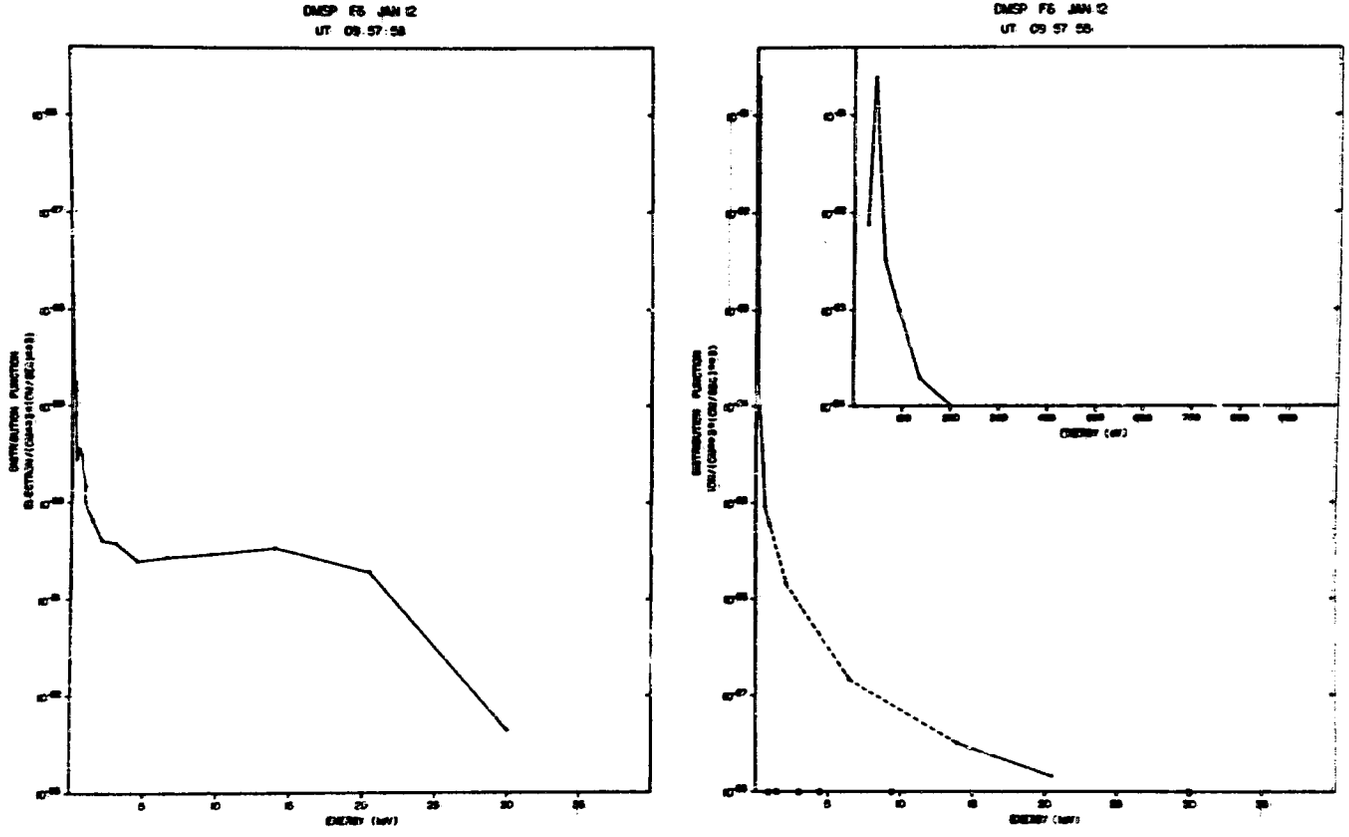

(e) At 09:57:58 UT.

Figure 6. – Continued.

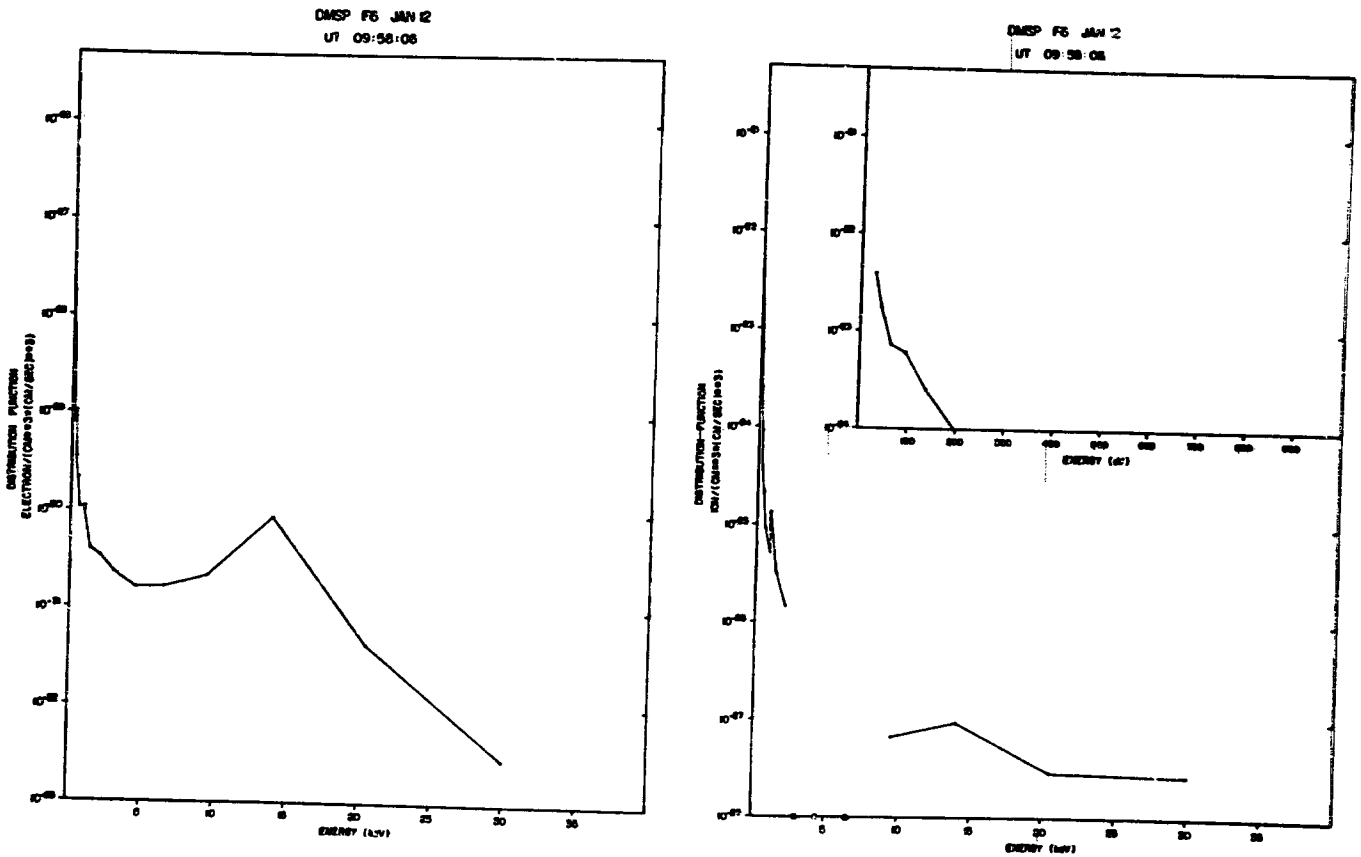

(f) At 09:58:06 UT.

Figure 6. - Concluded.

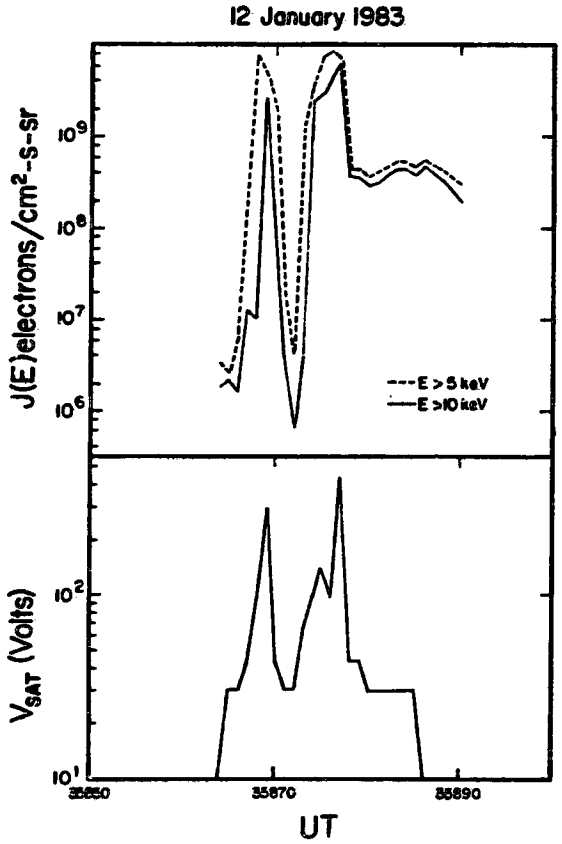

Figure 7. - Integral flux of electrons with energies >5 keV and >10 keV in the poleward inverted-V structure. The bottom panel gives the measured satellite potential as determined from charging peaks in the ion distribution functions at 1-sec intervals.

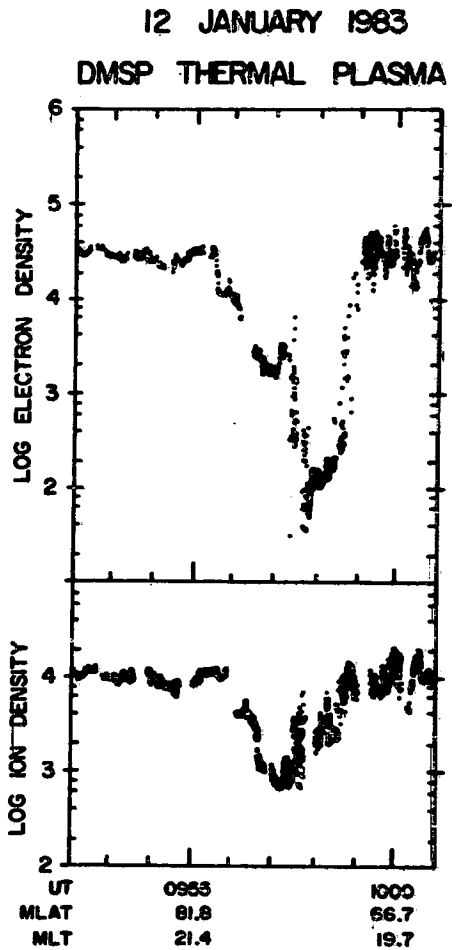

Figure 8. - Densities of thermal electrons and ions measured by DMSP/F6 in the vicinity of the inverted-V structure, in which large spacecraft potentials were detected.